AAAS

Science

30 APRIL 2026

BUILT TO SCALE

The power law behind how deltas grow p. 493

DELTAS

Apparent Hack's law in river deltas

Tian Y. Dong[1]*, Lawrence Vulis[2], Hongbo Ma[3]*, Alejandro Tejedor[4,5,2], Timothy A. Goudge[6]

River deltas are densely populated, ecologically vital landscapes threatened by rising sea levels. Distributary channel networks disperse sediment to build deltaic land, yet the relationship between the network organization and land building remains elusive. Inspired by Hack's law, which shows that watershed drainage area scales with channel length in tributary networks, we analyzed a global dataset of distributary networks and found a nearly identical scaling relationship between distributary channel length and nourishment area, the land-building counterpart to drainage area. Despite this apparent global scaling, we further identified two distinct local land-building patterns: uniform delta networks consistently follow Hack's law, whereas composite delta networks exhibit a scale break, transitioning from space-filling growth around the delta apex to quasi-linear growth near the coast. The unexpected growth patterns suggest that global simplicity and local variability coexist in how river deltas grow and organize.

River deltas are densely populated landscapes with critical socioeconomic and ecological functions (*1*–*4*), hosting ~4.5% of the world's population in only 0.5% of its land area (*5*). However, human and natural forcings, such as upstream damming and rising sea levels, have negatively affected land building in deltas (*6*–*10*). Distributary channel networks, widely found in river deltas, enable the dispersal of sediment and organic matter from the upstream river to a much larger area downstream, building deltaic land (*9*–*14*). The deltaic region where sediment deposits, downstream of a network apex (e.g., bifurcation node), is known as a nourishment area (*11*–*13*), a counterpart to the drainage area in tributary basins, where flow accumulates (Fig. 1A). Distributary channels and islands within nourishment areas are mainly built through processes such as over-levee floods and channel branching (*15*–*18*). Whereas it is straightforward to hypothesize that the network organization is linked to land building, the quantitative relationship between distributary characteristics, such as channel length and nourishment area, is not well understood, even though such a relationship could serve as a helpful rule of thumb for land-building estimation. Prior research has sought to scale the nourishment area (A) with the longest distributary channel length (L) (*11*, *13*), primarily using the results from numerical models. The scarcity of field observations has limited our understanding of the network-nourishment relationship. Delineating A in low-lying environments, such as deltas, is challenging, even with topographic data (Fig. 1A) (*11*, *12*). This is because low-relief topography makes the boundaries between neighboring nourishment areas extremely subtle. Such boundaries are theorized to be set by the merging of over-channel, divergent flows in interchannel island areas (*12*), rendering them difficult to measure globally (*19*).

In contrast, a scaling relationship is well established in geometrically similar tributary channel networks (Fig. 1A): Hack's law (*20*, *21*) defines a power law relation between the length of the longest tributary river (L_t) and the area of the associated drainage basin (A_t), $L_t = \alpha A_t^h$, where α and h are the empirical coefficient and exponent, respectively. Hack (*20*) observed α =1.4 and $h = 0.6$ for tributary river networks along the US East Coast, whereas subsequent studies (*22*) have shown h values ranging from 0.5 to 0.7, influenced by basin size (*22*) and shape (*23*), geology (*23*), and climate (*24*, *25*). Geometrically, $h = 0.5$ indicates space-filling growth, where the channel network grows evenly in both the down and cross (transverse) valley directions (*20*–*24*). In contrast, $h > 0.5$ indicates preferential down-valley growth, forming elongated basins (*20*–*24*). Moreover, the case when $h \sim 1$ indicates a linear relationship between channel length and basin area (*20*–*22*). Although theoretical explanations for Hack's law span concepts ranging from directed random walks (*22*) to optimal network theory (*21*, *26*), the physical controls remain debated and have been attributed to internal factors such as channel erosional processes through sediment transport (*27*) and external factors (*22*) such as tectonic history (*28*).

Numerous efforts have been made to understand the land-building processes of river deltas through mechanisms such as over-levee flow dispersion (*15*) and channel branching and avulsion (*16*–*18*) and through metrics such as shoreline roughness (*29*). Yet, despite the geometric parallels between distributary and tributary networks, existing relations between the distributary network (approximated by L) and the nourishment area remain inconclusive (*11*, *13*), largely because these relations are based on only two small-scale field deltas (<150 km^2 in area; mean $h = 0.53$) (*11*). Moreover, numerically simulated and laboratory-scale deltas yield different scaling exponents (mean h = 0.76 and 0.38, respectively; table S1) (*11*, *13*), and some exhibit multiscaling (i.e., curved data clouds), complicating interpretation (*13*). These seminal efforts, and their discrepancies, motivate our global field-scale analysis to determine whether the previously reported variability in A-to-L relationships is representative of a larger, more diverse set of field deltas, or whether a unified relationship analogous to Hack's law also emerges at the field scale. Specifically, we analyzed a comprehensive global dataset of 30 distributary networks spanning a range of scales and hydrodynamics (Fig. 1B and table S2) (*30*, *31*). Below, we show that our analysis has revealed unexpected insights into the deltaic land-building patterns driven by their distributary networks.

Hack's law in distributary channel networks of global river deltas

A fundamental challenge in quantifying deltaic land-building processes globally is the difficulty of systematically identifying nourishment areas. We addressed this gap by leveraging an existing graph-theory framework to consistently delineate 5892 nourishment areas across 30 distributary networks, enabling the first large-scale test of the scaling relationship between nourishment area and the longest associated distributary channel length among real-world deltas (Fig. 1B) (*30*, *31*). In this framework, each distributary network is represented as a directed acyclic graph (*3*), where nodes correspond to bifurcations, confluences, and outlets, and edges represent channels with assigned water and sediment flow directions, based on delta gradient and limited field measurements (Fig. 1C) (*31*, *32*). This graph-based approach enabled us to systematically define the nourishment network for each bifurcation, referred to as the nourishment apex (*14*), which comprises all downstream nodes and channels. The longest channel path from the nourishment apex to the coast was then extracted and measured (see details in the supplementary materials; Fig. 1C and fig. S1), and the nourishment area was estimated by summing the areas of the channel and interchannel regions within the nourishment network. To constrain uncertainty, we calculated three nourishment areas using three different local channel width (b) buffers—0×, 1×, 2× b (Fig. 1D)—and

[1]School of Earth, Environmental, and Marine Sciences, University of Texas Rio Grande Valley, Edinburg, TX, USA. [2]Department of Civil and Environmental Engineering, University of California, Irvine, Irvine, CA, USA. [3]Ven Te Chow Hydrosystems Laboratory, Department of Civil and Environmental Engineering, University of Illinois at Urbana-Champaign, Urbana, IL, USA. [4]Institute for Biocomputation and Physics of Complex Systems (BIFI), Universidad de Zaragoza, Zaragoza, Spain. [5]Department of Theoretical Physics, University of Zaragoza, Zaragoza, Spain. [6]Department of Earth and Planetary Sciences, Jackson School of Geosciences, The University of Texas at Austin, Austin, TX, USA. *Corresponding author. Email: tian.dong@utrgv.edu (T.Y.D.); hongboma@illinois.edu (H.M.)

used the mean value for our subsequent analyses (fig. S1) (*32*, *33*). This approach accounts for observed floodplain advection limits of bed material, such as fine to medium sand and flocculated mud (grain size: ~62.5 to 350 μm) (*33*, *34*), which are the building blocks of deltaic land (Fig. 1D) (*33*–*35*). The perimeter of the nourishment area at the coast was defined using previously mapped subaerial shorelines (Fig. 1C) (*30*, *31*). Although the graph-theory approach enabled us to map numerous *A*-and-*L* pairs consistently, it assumes unidirectional flow and therefore does not explicitly examine the bidirectional flow paths and sedimentation due to waves and tides (*14*). Nevertheless, the observed channel and nourishment area morphology reflects these marine influences, so they are implicitly incorporated into our analyses and may introduce variability (*14*, *30*). Additionally, although subaqueous delta channel networks are known to be part of deltaic progradation (*36*), they remain difficult to measure without detailed bathymetric data. For the scope of this work, we focused on the subaerial delta, which is both more readily mapped and more societally relevant. Given the above mapping and uncertainty-constraining techniques, the nourishment areas measured herein represent a conservative geometric estimate of subaerial deltaic land area nourished by riverine bed material on a decadal timescale (*4*, *12*, *15*, *19*, *35*).

We found a global power law relationship as follows (Fig. 2A)

$$L = 1.43 \pm^{0.22}_{0.19} A^{0.60 \pm 0.018} \quad (1)$$

The exponent and coefficient (±95% confidence intervals) of this global relation are remarkably similar to Hack's law (*20*): $L_t = 1.44A_t^{0.6}$. We also explored a normalized relationship between A and L to compare across delta size, such that A was normalized to the delta area, and L

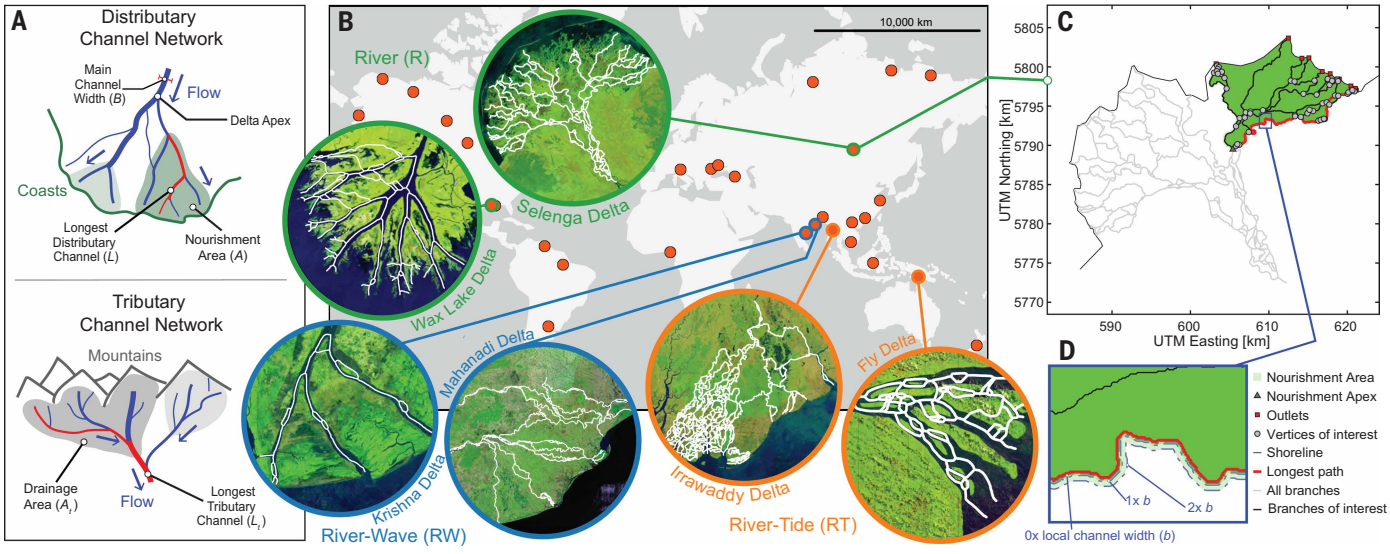

Fig. 1. Global river delta networks and nourishment areas. (**A**) Conceptual models illustrate the similarity between distributary deltas and tributary rivers in terms of channel networks. Here, *B* is the main channel width, measured upstream of the first bifurcation near the delta apex. *L* is the longest distributary channel, and *A* is the nourishment area. Similarly, L_t is the longest tributary channel, and A_t is the drainage area. (**B**) The dataset of deltas (*30*,*31*) used in this study covers a range of hydrodynamics, sizes, geography, valley confinement, and climate (*37*,*47*). (**C**) The delineation of the nourishment area and the longest distributary channel are shown in the example of the Selenga River delta (*32*,*40*,*50*). UTM, Universal Transverse Mercator. (**D**) Detailed view of the uncertainty range for the perimeter of the nourishment area. Here, *b* is the local channel width used to buffer the perimeter from 0 to 2× *b*, accounting for measurement uncertainties in the area and length of distributaries; see details in the main text and supplementary materials.

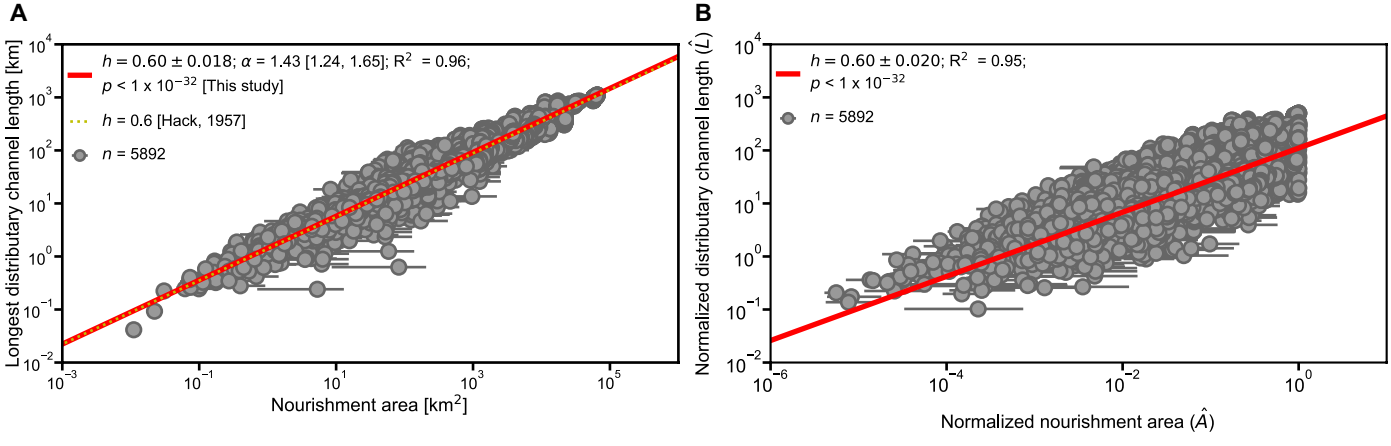

Fig. 2. The scaling between distributary channel length and nourishment area in global river deltas. (**A**) Dimensional and (**B**) dimensionless (*11*) scaling law of the distributary channel network of nourishment area and the length of the longest distributary channel in that area, obtained from 5892 measurements across 30 deltas. Parameter *n* is the number of data points used for the regression. R^2 and *P* values are reported. Error bars represent the range of *A*, among 0×, 1×, and 2× the local channel width, as shown in the buffer area boundary. Hack's law is shown in (A) as a yellow dotted line, for comparison.

was normalized by the main channel width (B), that is, the river's width measured upstream of the first bifurcation near the delta apex (Fig. 2B) (*11*). Still, the resultant scaling exponent for this robust [coefficient of determination (R^2) = 0.95] dimensionless relation ($h = 0.6 \pm 0.020$) remains the same as the dimensional form, indicating that delta nourishment areas follow a constant length-to-area scaling across nearly six orders of magnitude of delta sizes (Fig. 2B). From a land-building perspective, delta nourishment areas globally are elongated ($h > 0.5$), suggesting a preferential downstream growth direction toward the receiving basins. Additionally, a detailed sensitivity analysis addressing the uncertainty in the nourishment area and channel length measurements demonstrates that our results remain consistent despite these uncertainties (see supplementary materials; table S3).

Apparent global Hack's law conceals two land-building patterns at the local scale

Although statistically rigorous, the dimensionless power law relation exhibits considerable variability, suggesting the presence of additional geometric relationships. We thus further examined the origin of such variability within individual deltas. We found two distinct deltaic land-building patterns among our 29 studied deltas (the Wairau delta was excluded from the subanalysis owing to limited measurements). One group, denoted as the uniform delta network, conforms well to the global scaling law and Hack's law of tributary networks ($h \sim 0.6$) across all nourishment area sizes ($h = 0.66 \pm 0.14$; 14 out of 29 deltas; Fig. 3, A and C, and figs. S2 and S3). For the second group of deltas (15 out of 29 deltas; Fig. 3, B and D, and figs. S4 and S5), denoted as the composite delta network, we observed a scale break. In other words, nourishment areas in composite delta networks do not have a single scaling factor (i.e., a single value of h) but instead have two different scaling exponents within a single individual delta network. The scaling exponent for nourishment areas downstream of the scale break—that is, near the shoreline—is close to linear ($L \sim A^1$), with $h_1 = 0.83 \pm 0.13$. In contrast, upstream of the break, near the delta apex, the exponent is closer to the square root ($L \sim A^{0.5}$), $h_2 = 0.53 \pm 0.28$ (Fig. 4A). The scaling relation derived from aggregating measurements from several composite deltas of different sizes conforms to Hack's law and is similar to the relationships observed in individual uniform delta networks, suggesting that composite networks are masked within the global trend, giving rise to the appearance of a universal scaling law (Fig. 3E). Still, the average is $h = 0.60 \pm 0.043$ (Fig. 3E).

In the absence of a robust process-based explanation, we propose possible geometric reasons for the distinction between uniform and composite delta networks. River deltas with uniform networks are often confined in valleys (8 out of 14 uniform delta networks, or 57%; data S1) (*37*). Recall that Hack's law in tributary networks arises mainly

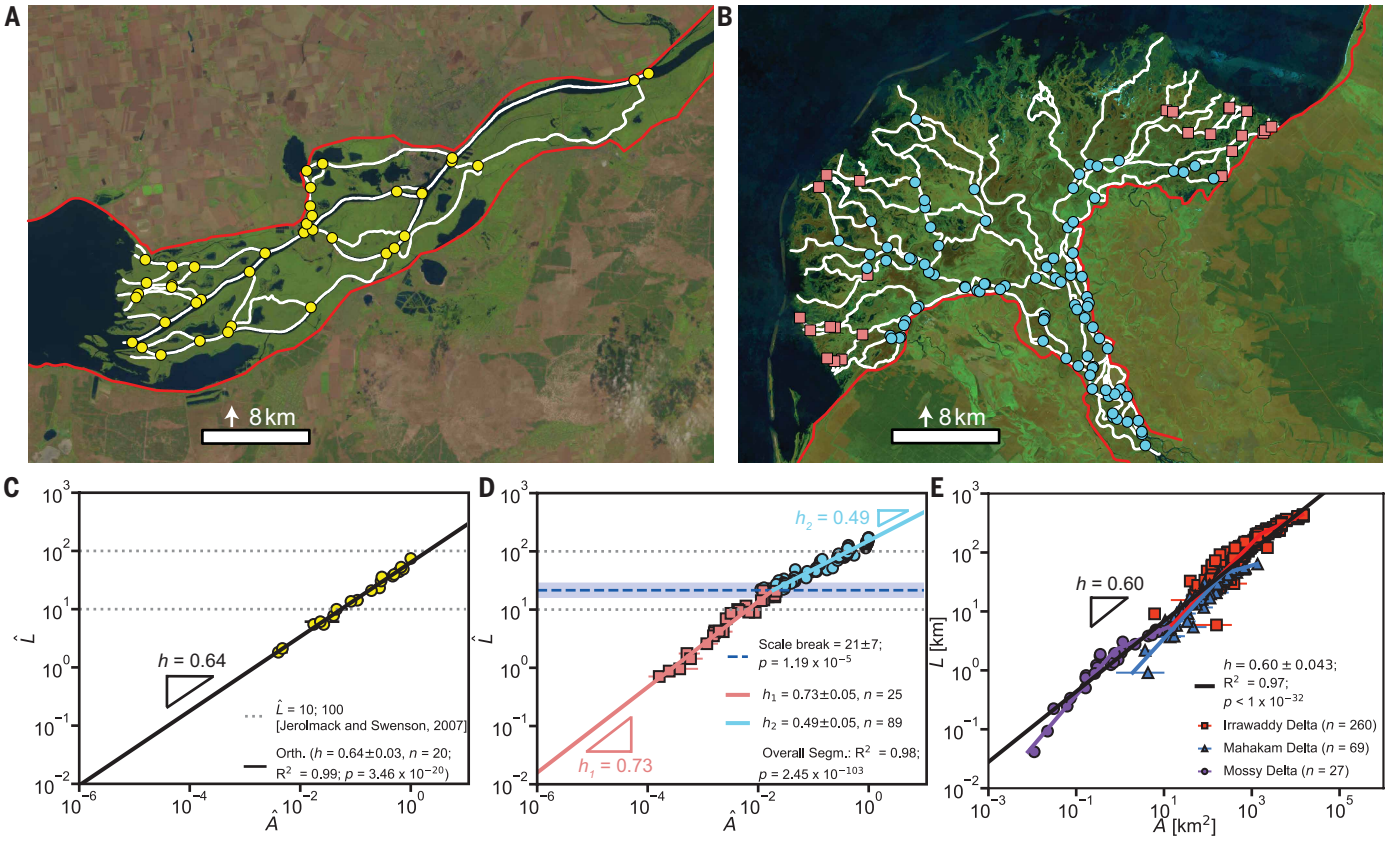

Fig. 3. Distinct deltaic land-building patterns for uniform and composite delta networks. Examples of uniform (**A**) and composite (**B**) delta networks: the Dnieper and Selenga deltas, respectively. Maps show the planform distribution of nourishment apexes (circles and squares) for each scaling regime. Red outlines indicate the extent of valley confinement (*37*, *47*), whereas white lines highlight the distributary channel network. (**C** and **D**) The corresponding scaling law of the normalized nourishment area ($\hat{A}$) versus the length of the longest distributary channel ($\hat{L}$), respectively, where the nourishment area is normalized by the delta area, and the channel width of the main branch normalizes the distributary channel length. Note that the scale break occurs at distances that are multiples of the channel width, separating the quasi-linear and square-root scaling regimes. (**E**) Dimensional scaling relations between channel length and nourishment area obtained by aggregating multiple composite delta networks of different sizes conform to Hack's law and are similar to those from individual uniform delta networks. R^2 and P values are reported. Parameter n is the number of data points used in the regressions. Error bars represent the range of A, among 0×, 1×, and 2× the local channel width, as shown in the buffer area boundary.

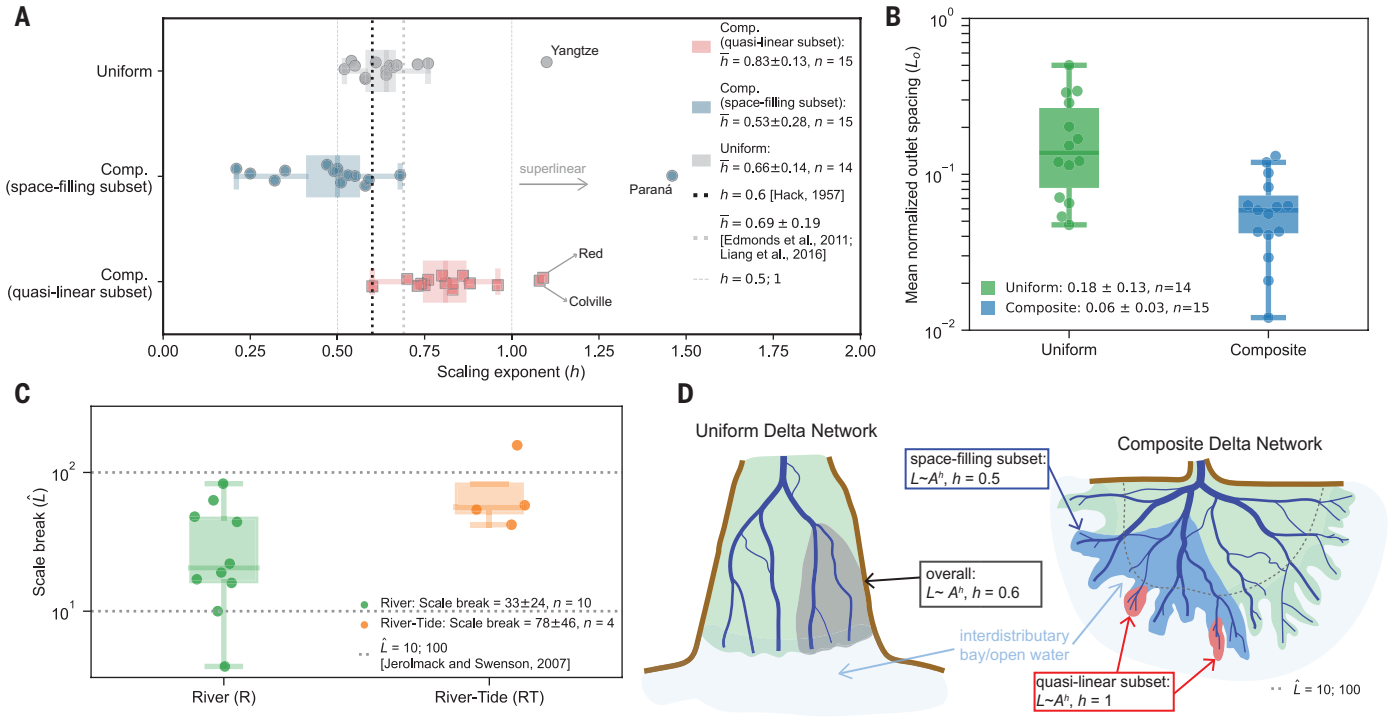

Fig. 4. Hydrodynamic conditions and distinct shoreline morphology for uniform and composite delta networks. (**A**) Scaling exponent *h* for the entire dataset for different channel network patterns. *n* is the number of data points. (**B**) Mean normalized outlet spacing (L_o) for river deltas with uniform and composite network patterns. (**C**) Locations of the scale break across hydrodynamics as a function of normalized channel length ($\hat{L}$). (**D**) Conceptual model summarizing the scaling law in river deltas with uniform and composite network patterns. Boxes in (B) and (C) indicate interquartile range (IQR, 75% to 25%), and lines inside the boxes are the medians. Whiskers and caps represent ±1.5× IQR.

because of a clear preferential flow direction from the tributary channels near the drainage divide to the basin outlet, following the basin's topographic gradient (slope). Moreover, per fractal and optimal network theories (*21*, *22*, *26*), the networks with a preferred flow direction, like directed random walk (*21*, *22*, *26*), will be optimized to have more down-valley flowing channels than transverse flowing channels to maximize drainage efficiency (*26*), so that the drainage basin is elongated ($h > 0.5$). We hypothesize that the above rationale is analogous to uniform delta networks, whereby the valley confinement sets a preferential flow direction from the delta apex to the valley exit near the coast, similar to topographic gradient in a drainage basin (*22*). The channel path that receives more flow undergoes greater erosion (*36*) and maintains this advantage as channels compete for discharge (*16*), thereby maximizing distributary efficiency for the distributary networks to grow toward the receiving basin ($h \sim 0.6$), similar to what is observed for tributary networks. Although the preferential down-valley path is prone to channel avulsion, the avulsed new path and subsequent development of a new distributary network would still be affected by the same constraint (valley confinement), contributing to elongated growth.

Composite delta networks, in contrast, are often unconfined (12 out of 15 composite delta networks, or 80%; data S1), and the channel networks have freedom to build across a broader range of flow directions and paths. Without confinement, delta channels, on average, grow radially toward the receiving basins and freely fill the space of the broad deltaic plain without major spatial restrictions, resulting in an overall fan shape. With sufficient sediment supply and hydrodynamics relative to the size of interchannel area (*4*, *11*, *15*, *16*, *19*), the nourishment area should follow $L \sim A^{0.5}$, indicating a free space–filling process (*22*) ($h \sim 0.5$), consistent with our observations of the upstream portion of composite delta networks ($h_2 = 0.53 \pm 0.28$).

As deltas prograde, distributary channels repeatedly bifurcate owing to mouth-bar deposition, which promotes splitting (*16*, *38*, *39*). With each bifurcation, water discharge is partitioned, and subordinate channels narrow (*16*, *32*, *40*), as the transverse sediment-spreading width between channel banklines and island edges (i.e., the nearest-edge distance), which represents the advection limit of overbank sediment, scales with channel width (*11*, *15*). Thus, the total sediment-spreading region of the narrowing channels cannot keep pace with the rapidly growing delta perimeter (i.e., the radially averaged subaerial shoreline) as the delta progrades. The growing gap between channels, coupled with preferential coarse-grained sedimentation near channel banklines (*12*, *15*, *36*), produces elongated strips of subaerial land. The resulting nourishment zones are elongated, driving *h* toward unity (*36*, *41*), consistent with our measurements in downstream composite delta networks ($h_1 = 0.83 \pm 0.13$).

These proposed geometric explanations are consistent with measurements of channel outlet spacing, which is expected to be closer in composite delta networks because of linearly protruding growth near the coastline. The Euclidean (exact, straight-line) distance between outlets was measured for each delta network and normalized by the sum of such distances to calculate the normalized outlet spacing (L_o; see supplementary materials). This metric, L_o, shows that outlets are three times more closely spaced for composite delta networks in comparison to uniform delta networks, with $L_o = 0.06 \pm 0.03$ and $L_o = 0.18 \pm 0.13$, respectively (Fig. 4B). These results further support the distinctions between the two network patterns, which have different characteristics of channel encroachment at the shoreline.

However, there are cases of uniform delta networks that can emerge from unconfined deltas (6 out of 14 uniform delta networks, or 43%; data S1). We hypothesize that this may be due to mechanisms that

inhibit the downstream protruding growth of the channel network and deltaic land building beyond the scale break, preventing the development of a composite delta network. For example, deltas with intense wave climates (four out of six unconfined uniform delta networks) often have only a few main branches because longshore wave current drives sediment transport to smooth the irregular deltaic shoreline and close river mouths (*42*), thereby constraining network growth even in unconfined deltas (*2*). Thus, we hypothesize that the quasi-linear growth region of the composite delta network is hindered under wave-influenced conditions, thereby eliminating the scale break and making the network appear uniform. A similar conceptual model of confinement has also been proposed to explain A and L relations derived from numerically simulated deltas (*13*) (Fig. 4A). In that model, the opening angle acts as a proxy for confinement, with a larger opening angle indicating less confinement, resulting in $L \sim A^{0.5}$ (*13*). Conversely, a smaller opening angle indicates more confined land growth, leading to relations closer to $L \sim A^{1}$ (*13*). In addition to marine influences, juvenile deltas may not yet have grown to a size where a scale break can occur (two out of six unconfined uniform delta networks), including Wax Lake (*12*, *19*, *36*) and the Mississippi River (most seaward region, known as the "bird's foot" or the La Balize lobe) deltas (*43*). These two deltas are about 0.05 thousand years (ka) and 0.5 to 1 ka in age, respectively (*12*, *43*), relative to the Holocene-aged (~7 to 10 ka) composite network Selenga delta (*32*, *40*).

The above geometric rationale also explains the spatial variation in the location of the scale break across different delta hydrodynamics. This break occurs around $(33 \pm 24)\times B$ for most river-dominated deltas, where scale breaks are measured as distance from the shoreline and normalized by B. River-dominated deltas typically form dendritic distributary networks, with bifurcations increasing downstream as mouth bars develop (*38*, *39*). Mouth bar–controlled distributaries have a characteristic length of ~10× the main channel width, on the basis of theory and observation (*38*, *39*). Because the transverse sediment spreading width remains ~2× the local channel width (*11*), each narrowing channel toward the coast produces a smaller nourishment area, consistent with $L \sim A^{1}$ (*36*, *41*) (Fig. 4C). In larger deltas, however, where channel length exceeds ~10× B, other processes such as avulsion and tidal influence dominate. Notably, avulsion length scales with the backwater length, which can exceed 100× B (*17*, *18*, *39*). Similarly, the scale break shifts more inland to $(78 \pm 46)\times B$ for river deltas with a strong tidal influence. We hypothesize that this reflects tidal hydrodynamics that keep channels open by transporting sediment landward along the valley axis ($h \sim 1$). As tidal forcing decreases landward, typically ~(10 to 100)× B from the coastline (*44*) (Fig. 4C), the riverine forcing (e.g., river floods) regains control and develops the transverse, cross-valley portion of the network, following the square-root scaling factor ($h \sim 0.5$).

In both uniform and composite delta networks, a few exceptional cases exhibit superlinear scaling relations ($h > 1$) (Fig. 4A), where the channel length grows faster, per unit, than the nourishment area. This superlinear behavior can arise under valley confinement, as in the Paraná delta, where a confined braided delta plain restricts area, while braiding increases channel length ($h = 1.46 \pm 0.02$; fig. S5). Similarly, in tide-dominated systems such as the Colville and Red deltas, tidal forcing promotes sinuosity and looping (*44*, *45*), causing distributary length to outpace area growth, again yielding $h > 1$ (figs. S4 and S5).

Implications of Hack's law in river deltas

By analyzing extensive real-world data, we confirmed a consistent power law relation between nourishment area and the longest channel length in river deltas, analogous to Hack's law in tributary networks, as previously hypothesized (*11*, *13*) (Fig. 4A). This global relation can serve as a rule of thumb for estimating deltaic land building when specific boundary conditions, such as diverse hydrodynamic influences (e.g., waves, tides), sediment type, and confinement, are unknown (*11*). Moreover, this framework can also inform restoration efforts and paleoenvironmental assessments. For example, by targeting interchannel areas within quasi-linear–scaling nourishment zones, the delta can transition more quickly into space-filling regimes. Also, given that delta size correlates with water and sediment supply (*1*–*4*, *18*), such scaling relationships, when paired with channel length and nourishment area measurements from paleo-delta deposits on Earth and Mars (*46*), could also be used to infer discharges, offering a novel tool for reconstructing past climates. Furthermore, this relation can also benchmark numerical and experimental deltas (*11*, *13*). However, this global simplicity may conceal local variability, such as scaling breaks, warranting caution when applying global findings to local contexts.

Despite the global A-L scaling, ~50% of deltas show local variability marked by a scale break (composite delta networks). In the absence of a process-based explanation, we propose a straightforward geometric rationale (Fig. 4D): Because river deltas maintain roughly stable dimensionless transverse sediment spreading width between channels and islands [i.e., nearest edge distance (*11*)], owing to similar advection length of over-bank sediment (*11*, *15*), wide trunk channels could entirely occupy space upstream, where shoreline and interchannel spacing are small. In contrast, downstream, the sediment spreading width of narrowing channels cannot keep pace with the expanding interchannel areas, leading to quasi-linear growth. This process does not apply to uniform delta networks, as the preferential flow direction will reshape the interchange island from the apex.

Scale breaks have also been observed in tributary networks, where scaling shifts reflect geologic controls. For example, h transitions from between ~0.62 and 0.67 in regional basins to between 0.5 and 1 in continental basins, and from advective channels ($h \sim 0.6$) to hillslope heads dominated by diffusion ($h \sim 1$) (*22*). By contrast, the channel tips of deltas are mostly subaqueous, limiting the availability of large datasets (*36*). Because our work focuses only on the subaerial delta, whether additional scale break(s) occur between subaerial and subaqueous delta networks remains unresolved and is an exciting avenue for future work. Furthermore, valley confinement plays a vital role in determining the complexity of the delta network, as others have shown, including hypsometry and delta slope (*47*). However, a physical understanding of how confinement affects river delta morphology remains lacking, which could lead to a process-based reasoning for the scale breaks. In addition, past work has shown that the nearest edge distance can vary in a delta (*48*), possibly because of tidal influences (*11*, *48*), which could help explain the location of scale breaks.

Our results raise the broader question of why river networks, from uppermost tributaries to the lowermost distributaries, share the same Hack's law (*11*, *13*, *22*, *49*). We may draw parallels between the two fields, which reveal universality within river network studies and help understand their common physics. For instance, we may ask questions such as where a delta channel truly begins (or ends), paralleling longstanding debates over channel heads in tributary systems (*50*). Future studies may also investigate whether additional delta network metrics, such as slope-area scaling, widely used in tributary systems, yield new insights into distributary organization.

REFERENCES AND NOTES

1. J. H. Nienhuis *et al.*, *Annu. Rev. Earth Planet. Sci.* **51**, 79–104 (2023).
2. J. H. Nienhuis *et al.*, *Nature* **577**, 514–518 (2020).
3. A. J. Hoitink *et al.*, *J. Geophys. Res. Earth Surf.* **125**, e2019JF005201 (2020).
4. D. A. Edmonds *et al.*, *Nat. Sustain.* **6**, 644–651 (2023).
5. D. A. Edmonds, R. L. Caldwell, E. S. Brondizio, S. M. O. Siani, *Nat. Commun.* **11**, 4741 (2020).
6. K. M. Sanks, J. B. Shaw, K. Naithani, *J. Geophys. Res. Earth Surf.* **125**, e2019JF005389 (2020).
7. J. P. M. Syvitski, C. J. Vörösmarty, A. J. Kettner, P. Green, *Science* **308**, 376–380 (2005).
8. S. H. Ensign, J. N. Halls, E. K. Peck, *Science* **382**, 1191–1195 (2023).
9. P. Passalacqua, *Geomorphology* **277**, 50–62 (2017).
10. A. Tejedor *et al.*, *Proc. Natl. Acad. Sci. U.S.A.* **114**, 11651–11656 (2017).

11. D. A. Edmonds, C. Paola, D. C. J. D. Hoyal, B. A. Sheets, *J. Geophys. Res. Earth Surf.* **116**, F04022 (2011).
12. J. B. Shaw, D. Mohrig, R. W. Wagner, *J. Geophys. Res. Earth Surf.* **121**, 372–391 (2016).
13. M. Liang, C. Van Dyk, P. Passalacqua, *J. Geophys. Res. Earth Surf.* **121**, 465–496 (2016).
14. A. Tejedor, A. Longjas, I. Zaliapin, E. Foufoula-Georgiou, *Water Resour. Res.* **51**, 3998–4018 (2015).
15. G. Salter, M. P. Lamb, *Geophys. Res. Lett.* **49**, e2022GL098885 (2022).
16. M. G. Kleinhans, R. I. Ferguson, S. N. Lane, R. J. Hardy, *Earth Surf. Process. Landf.* **38**, 47–61 (2013).
17. S. Brooke *et al.*, *Science* **376**, 987–990 (2022).
18. V. Ganti, A. J. Chadwick, H. J. Hassenruck-Gudipati, B. M. Fuller, M. P. Lamb, *Sci. Adv.* **2**, e1501768 (2016).
19. K. Wright, J. Hariharan, P. Passalacqua, G. Salter, M. P. Lamb, *J. Geophys. Res. Earth Surf.* **127**, e2022JF006769 (2022).
20. J. T. Hack, "Studies of longitudinal stream profiles in Virginia and Maryland," US Geological Survey Professional Paper 294-B (US Government Printing Office, 1957); https://doi.org/10.3133/pp294B.
21. R. Rigon *et al.*, *Water Resour. Res.* **32**, 3367–3374 (1996).
22. P. S. Dodds, D. H. Rothman, *Annu. Rev. Earth Planet. Sci.* **28**, 571–610 (2000).
23. T. Sassolas-Serrayet, R. Cattin, M. Ferry, *Nat. Commun.* **9**, 3791 (2018).
24. R. S. Yi, Á. Arredondo, E. Stansifer, H. Seybold, D. H. Rothman, *Proc. R. Soc. London Ser. A* **474**, 20180081 (2018).
25. W. Luo, A. D. Howard, R. A. Craddock, E. A. Oliveira, R. S. Pires, *Geophys. Res. Lett.* **50**, e2022GL102604 (2023).
26. R. Rigon, A. Rinaldo, I. Rodriguez-Iturbe, R. L. Bras, E. Ijjasz-Vasquez, *Water Resour. Res.* **29**, 1635–1646 (1993).
27. J. T. Perron, P. W. Richardson, K. L. Ferrier, M. Lapôtre, *Nature* **492**, 100–103 (2012).
28. Q. Li, N. M. Gasparini, K. M. Straub, *Geology* **46**, 407–410 (2018).
29. L. Vulis *et al.*, *Geophys. Res. Lett.* **50**, e2022GL102684 (2023).
30. J. Hariharan, A. Piliouras, J. Schwenk, P. Passalacqua, *Geophys. Res. Lett.* **49**, e2022GL097897 (2022).
31. J. Schwenk, A. Piliouras, J. C. Rowland, *Earth Surf. Dyn.* **8**, 87–102 (2020).
32. T. Y. Dong *et al.*, *Water Resour. Res.* **56**, e2020WR027199 (2020).
33. J. A. Nghiem *et al.*, *J. Geophys. Res. Earth Surf.* **130**, e2025JF008366 (2025).
34. M. Kim, B. Chun, E. Chamberlain, W. Kim, *Sedimentology* **72**, 165–188 (2025).
35. J. A. Nittrouer, J. Shaw, M. P. Lamb, D. Mohrig, *Geol. Soc. Am. Bull.* **124**, 400–414 (2012).
36. J. B. Shaw, D. Mohrig, *Geology* **42**, 31–34 (2014).
37. O. A. Prasojo, T. B. Hoey, A. Owen, R. D. Williams, *Geophys. Res. Lett.* **49**, e2021GL093656 (2022).
38. D. A. Edmonds, R. L. Slingerland, *J. Geophys. Res. Earth Surf.* **112**, F02034 (2007).
39. D. J. Jerolmack, J. B. Swenson, *Geophys. Res. Lett.* **34**, 2007GL031823 (2007).
40. T. Y. Dong *et al.*, *Geol. Soc. Am. Bull.* **128**, 1297–1312 (2016).
41. W. T. Ke, J. B. Shaw, R. C. Mahon, C. A. Cathcart, *J. Geophys. Res. Earth Surf.* **124**, 1878–1898 (2019).
42. J. H. Nienhuis, A. D. Ashton, L. Giosan, *Geology* **43**, 511–514 (2015).
43. J. M. Coleman, H. H. Roberts, G. W. Stone, *J. Coast. Res.* **14**, 699–716 (1998).
44. A. F. Hoitink, D. A. Jay, *Rev. Geophys.* **54**, 240–272 (2016).
45. A. Konkol, J. Schwenk, E. Katifori, J. B. Shaw, *Geophys. Res. Lett.* **49**, e2022GL098284 (2022).
46. R. A. DiBiase, A. B. Limaye, J. S. Scheingross, W. W. Fischer, M. P. Lamb, *J. Geophys. Res. Planets* **118**, 1285–1302 (2013).
47. J. B. Shaw, K. M. Sanks, A. Piliouras, *Geol. Soc. Am. Bull.* **138**, 342–350 (2025).
48. P. Passalacqua, S. Lanzoni, C. Paola, A. Rinaldo, *J. Geophys. Res. Earth Surf.* **118**, 1838–1849 (2013).
49. J. M. Swartz, B. T. Cardenas, D. Mohrig, P. Passalacqua, *Nat. Geosci.* **15**, 216–221 (2022).
50. D. R. Montgomery, W. E. Dietrich, *Nature* **336**, 232–234 (1988).
51. T. Dong, L. Vulis, H. Ma, A. Tejedor, T. Goudge, Apparent Hack's Law in River Deltas [Data set], Zenodo (2025); https://doi.org/10.5281/zenodo.17029586.

ACKNOWLEDGMENTS

We thank the Earth Surface Processes Institute, run by the Community Surface Dynamics Modeling System (CSDMS), for connecting T.Y.D. and L.V. to conceptualize this work. We are grateful to P. Passalacqua and two anonymous reviewers for their insightful comments, which substantially improved the quality of this manuscript. **Funding:** This work was supported by National Science Foundation Division of Earth Sciences Postdoctoral Fellowship 1952814 (T.Y.D.); the University of California Lab Fees in Residence Graduate Fellowship Grant L21GF3569 (L.V.); National Aeronautics and Space Administration Earth and Space Science Fellowship Grant 338-80NSSC18K1409 (L.V.); National Science Foundation Division of Earth Sciences Grant 2342937 (A.T.); National Science Foundation Division of Research, Innovation, Synergies and Education Grant 2425748 (A.T.); and Ministerio de Ciencia, Innovación y Universidades, Agencia Española de Investigación Grant PID2023-149409NB-I00 (A.T.).
Author contributions: Conceptualization: T.Y.D., L.V., H.M.; Methodology: T.Y.D., L.V., A.T.; Investigation: T.Y.D., L.V., H.M.; Visualization: T.Y.D.; Funding acquisition: T.Y.D., L.V., H.M., A.T., T.A.G.; Project administration: T.Y.D.; Supervision: T.Y.D., H.M., T.A.G.; Writing – original draft: T.Y.D.; Writing – review & editing: T.Y.D., L.V., H.M., A.T., T.A.G.. **Competing interests:** The authors declare that they have no competing interests. **Data, code, and materials availability:** All data analyzed in this study are tabulated in the supplementary materials and the associated Python codes are archived in Zenodo (*51*). The satellite imagery shown in Figs. 1 and 3 is publicly available, namely, US Geological Survey (USGS)/National Aeronautics and Space Administration Landsat satellite imagery, which can be downloaded from the USGS Earth Explorer (https://earthexplorer.usgs.gov/). Delta channel networks and shorelines used in this study are available in (*30*, *31*). This study did not generate new samples or physical materials.

SUPPLEMENTARY MATERIALS

science.org/doi/10.1126/science.ady6805
Materials and Methods; Figs. S1 to S33; Tables S1 to S3; References (*52*–*55*); Data S1 to S3

Submitted 30 April 2025; accepted 18 February 2026

10.1126/science.ady6805

Apparent Hack's law in river deltas

Tian Y. Dong, Lawrence Vulis, Hongbo Ma, Alejandro Tejedor, and Timothy A. Goudge

Science **392** (6797), . DOI: 10.1126/science.ady6805

Editor's summary
A river's branching tributary network follows a power-law scaling relationship called Hack's law, in which the area of a drainage basin can be predicted by the length of its longest tributary channel. At a river's delta, distributary channels disperse in a similarly fractal way, yet a comparable scaling relationship has been elusive. Looking globally, however, Dong *et al*. extracted a nearly identical power-law relationship between distributary channel length and a delta's land-building area. A Hack's law for deltas that has defined local scaling variability provides a formula for understanding how deltas grow, change, and can be restored. —Angela Hessler